See related commentary on pg 4

A Guide to Studying Human Hair Follicle Cycling In Vivo

Ji Won Oh[1,2,3,4,5], Jennifer Kloepper[6], Ewan A. Langan[6,7], Yongsoo Kim[8], Joongyeub Yeo[9], Min Ji Kim[10], Tsai-Ching Hsi[3,4,5], Christian Rose[11], Ghil Suk Yoon[12], Seok-Jong Lee[10], John Seykora[13], Jung Chul Kim[1,2], Young Kwan Sung[2], Moonkyu Kim[1,2,16], Ralf Paus[14,15,16] and Maksim V. Plikus[3,4,5,16]

Hair follicles (HFs) undergo lifelong cyclical transformations, progressing through stages of rapid growth (anagen), regression (catagen), and relative "quiescence" (telogen). Given that HF cycling abnormalities underlie many human hair growth disorders, the accurate classification of individual cycle stages within skin biopsies is clinically important and essential for hair research. For preclinical human hair research purposes, human scalp skin can be xenografted onto immunocompromised mice to study human HF cycling and manipulate long-lasting anagen in vivo. Although available for mice, a comprehensive guide on how to recognize different human hair cycle stages in vivo is lacking. In this article, we present such a guide, which uses objective, well-defined, and reproducible criteria, and integrates simple morphological indicators with advanced, (immuno)-histochemical markers. This guide also characterizes human HF cycling in xenografts and highlights the utility of this model for in vivo hair research. Detailed schematic drawings and representative micrographs provide examples of how best to identify human HF stages, even in suboptimally sectioned tissue, and practical recommendations are given for designing human-on-mouse hair cycle experiments. Thus, this guide seeks to offer a benchmark for human hair cycle stage classification, for both hair research experts and newcomers to the field.

Journal of Investigative Dermatology (2016) **136,** 34-44; doi:10.1038/JID.2015.354

INTRODUCTION

Limitations of the murine hair follicle model

Human and murine hair follicles (HFs) share the same essential features of organization and function, and basic hair research in mice has long been both the foundation and at the forefront of our understanding of hair biology (Dry, 1926; Hsu et al., 2014; Montagna and Ellis, 1958; Plikus and Chuong, 2014; Schneider et al., 2009; Sundberg et al., 2005). In both species, HFs contain the same principal cell types and undergo repetitive cycling, alternating between the phases of active growth (anagen), regression (catagen), and relative "quiescence" (telogen) (Geyfman et al., 2014; Paus and Cotsarelis, 1999; Schneider et al., 2009).

However, significant interspecies differences exist, limiting the translational potential of the murine HF model. Critically, anagen in the human scalp lasts for several years, whereas murine dorsal skin anagen is only 2−3 weeks long (Garza et al., 2012; Halloy et al., 2000; Müller-Röver et al., 2001), and epithelial HF stem cells differ in their markers and characteristics (Cotsarelis, 2006; Kloepper et al., 2008; Purba et al., 2014). Furthermore, whereas murine pelage HFs synchronize their cycles and grow in coordinated domains (Plikus et al., 2008, 2011), human scalp HFs cycle asynchronously (mosaic, stochastically driven hair cycle) (Dawber, 1997; Halloy et al., 2000) (see also Supplementary Text S1 online).

Although both human and murine HFs are exquisitely responsive to hormonal stimulation, their responses differ. For example, although estrogens and prolactin inhibit murine HF growth and cycling, both hormones prolong anagen duration in human female temporofrontal scalp HFs (Langan et al., 2010; Ohnemus et al., 2006). Thus, the response of murine HFs to stimulation with candidate hair growth-modulating agents does not necessarily predict how human HFs will respond, and may actually be misleading. Finally, the characteristic phenomenon of androgen-dependent HF miniaturization, seen in androgenetic

[1]*Hair Transplantation Center, Kyungpook National University Hospital, Daegu, Korea;* [2]*Department of Immunology, Kyungpook National University School of Medicine, Daegu, Korea;* [3]*Department of Developmental and Cell Biology, University of California, Irvine, Irvine, California, USA;* [4]*Sue and Bill Gross Stem Cell Research Center, University of California, Irvine, Irvine, California, USA;* [5]*Center for Complex Biological Systems, University of California, Irvine, Irvine, California, USA;* [6]*Department of Dermatology, University of Lübeck, Lübeck, Germany;* [7]*Comprehensive Centre for Inflammation Research, University of Lübeck, Germany;* [8]*Division of Molecular Pathology, the Netherlands Cancer Institute, Amsterdam, the Netherlands;* [9]*Institute for Computational and Mathematical Engineering, Stanford University, Stanford, California, USA;* [10]*Department of Dermatology, Kyungpook National University School of Medicine, Daegu, Korea;* [11]*Dermatohistologisches Labor Rose/Bartsch, Lübeck, Germany;* [12]*Department of Pathology, Kyungpook National University School of Medicine, Daegu, Korea;* [13]*Department of Dermatology, University of Pennsylvania, Philadelphia, Pennsylvania, USA;* [14]*Dermatology Research Centre, Institute of Inflammation and Repair, University of Manchester, Manchester, UK; and* [15]*Department of Dermatology, University of Münster, Münster, Germany*

[16] *These authors contributed equally to this work.*

Correspondence: Moonkyu Kim, Department of Immunology, Kyungpook National University School of Medicine, Daegu, Korea. E-mail: moonkim@knu.ac.kr or Ralf Paus, Dermatology Research Centre, Institute of Inflammation and Repair, University of Manchester, Manchester M13 9PL, UK. E-mail: ralf.paus@manchester.ac.uk or Maksim V. Plikus, Department of Developmental and Cell Biology, University of California, Irvine, Irvine, California 92697, USA. E-mail: plikus@uci.edu

Abbreviations: DP, dermal papilla; HF, hair follicles; IRS, inner root sheath; HF-IS, human scalp skin in situ; HF-XG, xenografted anagen HF; SCID, severe combined immunodeficiency

Received 25 February 2015; revised 19 August 2015; accepted 24 August 2015; accepted manuscript published online 9 September 2015

© 2015 The Authors. Published by Elsevier, Inc. on behalf of the Society for Investigative Dermatology.

alopecia (Dawber, 1997; Lattanand and Johnson, 1975), is not reproducible in the currently available mouse strains (Crabtree et al., 2010; Nakamura et al., 2013; Sundberg et al., 1999).

The clinical importance of standardized human hair cycle staging

Considering that scalp skin harbors approximately 100,000 terminal HFs, even minor variations in their cycling have major clinical effects (Dawber, 1997). Thus, a small increase in the percentage of telogen scalp HFs by just a few percent can cause substantial effluvium, for example, because of premature catagen induction by hormones, inflammatory mediators, neuropeptides, autoimmune reactions, cytotoxic drugs, psychoemotional stress, or malnutrition (reviewed in Atanaskova Mesinkovska and Bergfeld, 2013; Dawber, 1997; Paus, 2006; Paus and Cotsarelis, 1999; Paus and Foitzik, 2004; Paus et al., 2013; Shapiro, 2007). Moreover, establishing an accurate anagen-to-catagen-to-telogen HF ratio is important for diagnosing the kind of alopecia at hand and for assessing its severity and progression. Although the telogen-to-anagen ratio can be determined noninvasively via a phototrichogram, skin biopsies and histological staging are required to identify catagen HFs and to distinguish defined anagen substages (Van Neste, 2002). Additionally, accurate histological hair cycle stage assessment is essential for quantitative preclinical and clinical hair research.

Therefore, an easy-to-follow objective guide for the precise, standardized, and reproducible identification of human HF cycle stages is needed, ideally on the basis of routine histochemistry alone, without having to examine stage-specific molecular markers by immunohistochemistry, unless the latter provides crucial, otherwise unobtainable, insights. Although a comprehensive guide for murine hair cycle staging has long been available (Müller-Röver et al., 2001), the only major review on the human hair cycle dates back to 1959 (Kligman, 1959), yet it provides insufficient detail to guide accurate hair cycle staging. Although this review has since been complemented by excellent atlases (e.g., Sperling et al., 2012; Whiting, 2004), and by a guide for evaluating the anagen-catagen transition of microdissected, organ-cultured human HFs ex vivo (Kloepper et al., 2010), a standardized, comprehensive, user-friendly, and electronically accessible human hair cycle guide in vivo is missing. This study strives to provide this.

Standardized assessment of human HF cycling in the xenograft mouse model

HF xenotransplantation is currently the only preclinical assay that permits complete human HF cycling and supports long-lasting human anagen studies in vivo. Therefore, it is a uniquely instructive and indispensable human hair research tool. However, despite several early reports (De Brouwer et al., 1997; Gilhar et al., 1988, 1998; Hashimoto et al., 2000, 2001; Jahoda et al., 1996; Krajcik et al., 2003; Lyle et al., 1999; Tang et al., 2002; Van Neste et al., 1989), and more recent uses for the experimental induction of alopecia areata (Gilhar et al., 2013), postgrafting human scalp hair cycle dynamics remain poorly characterized, hindering broader adaptation of this model. Furthermore, as xenografting is inevitably associated with surgery-, wound healing-, reinnervation-, and reperfusion-related phenomena that are absent during normal scalp HF cycling in vivo (see below), a detailed morphological comparison between xenografted and freshly biopsied human scalp HFs is needed. Because such a comparison has previously been unavailable, there is limited understanding of the extent to which human hair cycle events seen in xenotransplants are representative of normal human hair cycle progression in vivo.

Therefore, this human hair cycle guide is complemented with a systematic analysis of HF cycling in xenografted human scalp skin, noting major similarities alongside minor differences and specific transplantation-related phenomena that one needs to be aware of. Finally, we report statistically validated, practical recommendations for designing human-on-mouse HF xenotransplantation experiments.

RESULTS

Human hair cycle staging

HF cycle stages were evaluated based on the following histological characteristics (Supplementary Table S1): (i) size and shape of the dermal papilla (DP) and hair matrix, (ii) epithelial outer root sheath (ORS) morphology, (iii) connective tissue sheath (CTS) and vitreous membrane morphology, (iv) hair shaft characteristics, such as length and the presence of club hair, (v) the presence of the inner root sheath (IRS), (vi) pigment distribution, and (vii) the presence of apoptotic and/or proliferating cells, following the example of murine hair cycle staging (Müller-Röver et al., 2001). Additional markers can be assessed immunohistologically to demarcate selected cell populations or structures, such as epithelial stem cells or HF-associated keratins, but are dispensable for hair cycle staging (Supplementary Table S2 online).

Similar to routine hair transplantation in humans (Unger, 2005) or in chemotherapy-induced alopecia (Hendrix et al., 2005; Paus et al., 2013), xenografted anagen HFs (HFs-XG) predominantly enter catagen, thereby inducing a new hair cycle and allowing for quick recovery from surgery-associated damage. Whereas these HFs-XG often show signs of dystrophy ("dystrophic catagen"), less damaged HFs-XG enter into the "dystrophic anagen" damage-response pathway, with retarded progression into a new hair cycle (Paus et al., 2013). In the following sections, we first describe HF morphology in human scalp skin in situ (HFs-IS) and subsequently explain the extent to which the hair cycle stages of HFs-XG recapitulate HFs-IS. Importantly, when staging HFs-IS, HF size and position relative to neighboring follicles and to epidermal/dermal or dermal/adipose tissue boundaries can be used as morphological landmarks. However, these landmarks cannot be recruited for hair cycle staging of HFs-XG, especially if follicular units (Unger, 2005) are transplanted.

Early catagen

This guide covers catagen first because after human HFs complete their fetal morphogenesis (Montagna and Ellis, 1958), their lifelong cycling activity begins with the first catagen entry in utero. For practical reasons, the eight distinct stages of catagen development in mice (Müller-Röver et al., 2001) are best subdivided into three relatively easily recognizable stages (Kloepper et al., 2010): "early catagen,"

equivalent to murine catagen phases I–IV; "mid-catagen" (i.e., murine catagen V–VI); and "late catagen" (i.e., murine catagen VII–VIII) (Müller-Röver et al., 2001).

In HFs-IS, matrix and DP volume reduction, together with a complete cessation of HF pigmentation, are the earliest signs of catagen development that can be positively distinguished from anagen stage VI. Characteristically, the DP becomes more condensed and almond-shaped. Termination of melanogenesis (Bodo et al., 2007; Slominski et al., 2005; Tobin, 2011) results in the proximal end of the hair shaft becoming notably less pigmented than in anagen VI HFs (Figure 1a). Some melanin incontinence into the DP can also be seen, as the normal transfer of melanosomes into precortical hair matrix keratinocytes is interrupted (Tobin, 2011) (Figure 1b, feature #5). Importantly, the morphology of the bulge region and the overall follicle length remain largely unchanged compared with anagen VI HFs-IS, and the lower HF portion rests below the dermal/adipose junction.

Positive staining for apoptotic cells (e.g., by activated caspase-3 or TUNEL immunofluorescence) in the regressing epithelium above the DP can be used as a definitive immunohistological marker of early catagen, because apoptotic cells are essentially undetectable in healthy anagen VI HFs in vivo (Botchkareva et al., 2006, 2007; Sharova et al., 2014). Furthermore, the downregulation of IRS and DP immunohistological markers can be used to differentiate early-catagen HFs from anagen VI HFs (see Supplementary Table S2) (Commo and Bernard, 1997; Malgouries et al., 2008a, 2008b).

In HFs-XG, anagen VI progresses into catagen unusually rapidly so that on day 2 after grafting, follicles that closely correspond to murine catagen stage IV (Müller-Röver et al., 2001) can already be found (Figure 1d–h). In catagen HFs-XG, the matrix is reduced down to just 2–3 cell layers, yet still envelops a small, almond-shaped DP (Figure 1f and g, feature #2). The newly forming club hair is located a short distance above the condensed DP (Figure 1f and g, feature #6).

A significant portion (76.4%) of HFs-XG undergo "dystrophic catagen" (Paus et al., 2013), during which a normal, serrated club hair shaft fails to form. In addition, the regressing hair matrix above the DP commonly contains ectopic melanin deposits (Supplementary Figures S1a–e and S3 online).

Mid-catagen

In HFs-IS and HFs-XG, the matrix and DP further decrease in volume; residual matrix is only 1–2 cell layers thick and only partially wraps around the condensed, almond-shaped DP (Figure 1i, features #1 and #2). A brush-like club hair becomes prominent at this stage, and it resides above the dermal/adipose boundary (Figure 1i and p, feature #4). The newly formed epithelial strand (the remnant of the regressing hair matrix and proximal ORS) between the club hair and the DP is thin, generally lacks pigment, and can have a ruffled, zipper-like appearance (Figure 1i, o, and p, feature #3). Compared with early-catagen, mid-catagen HFs acquire visible thickening of the vitreous membrane of the CTS, which prominently stains for the glycoprotein, biglycan (Figure 1i, o, and q, feature #5). Because the IRS regresses and disappears during catagen, its absence can be used to differentiate mid- to late-catagen HFs from early-anagen III HFs on hematoxylin and eosin stained sections (Commo and Bernard, 1997). Dystrophic mid-catagen HFs-XG either lack or have incompletely formed club hairs, and in these HFs melanin clumps and vitreous membrane thickening are prominent (Supplementary Figures S1f–j and S3).

Late catagen

In both HFs-IS and HFs-XG, the matrix disappears, and the DP becomes condensed and ball-shaped (Figure 1r and y, feature #1). The club hair is now prominently visible (Figure 1r and z, feature #4), and the epithelial strand is shortened (to about half the length of that of mid-catagen HFs) (Figure 1r, x, and y, feature #3). The thickened CTS, which characteristically trails below the DP into the adipose tissue in HFs-IS and can contain melanin clumps (in HFs-XG), becomes prominent at this stage ("dermal streamer") (Figure 1r, feature #5). A few apoptotic cells can still be detected in the epithelial strand (Figure 1t, feature #6). Importantly, in late catagen, apoptotic cells can also be found in the shrinking sebaceous gland (Figure 1t, feature #7), like in mice (Lindner et al., 1997). Dystrophic late catagen HFs-XG display ectopic melanin deposition in the epithelium (Supplementary Figures S1k–o and S3) and prominent pleats in the bulge region (Figure 1x, feature #8), which colocalize with CD200-positive epithelial progenitors (Figure 1z) (Purba et al., 2014).

Telogen

HFs with typical telogen morphology can be seen in situ, but are generally absent in xenografts. Their defining characteristics are: (i) positioning of the HF entirely above the dermal/adipose boundary (Figure 2a, feature #4), (ii) prominent unpigmented, serrated club hair (Figure 2a, feature #3), and (iii) very compact, well-rounded DP separated from the club hair by a maximally shortened, unpigmented epithelial strand, the "secondary hair germ" (Figure 2a, features #1 and #2). Apoptotic cells are generally not observed (Figure 2c, feature #5).

However, consistent with previous reports (reviewed in Geyfman et al., 2014), a few dispersed (not clustered) proliferating cells can often be seen in the secondary hair germ and the distal epithelium of telogen HFs-IS (Figure 2c, feature #6). Thus, telogen HFs are not really "resting." Unfortunately, the functionally crucial distinction between "refractory" and "competent" telogen HFs is not possible by histology, and the corresponding molecular signatures have only been characterized for murine telogen (see Geyfman et al., 2014). Importantly, human telogen HFs-IS can undergo exogen, the phase of active club hair shedding (Higgins et al., 2009; Stenn, 2005). Following exogen, HFs-IS enter kenogen, the telogen phase without the presence of a club hair (Rebora and Guarrera, 2002), which can last for several months (Courtois et al., 1994).

Anagen I

Because of their relatively short duration, early stages of anagen can be quite difficult to identify in situ. One also needs to keep in mind that hair cycle staging describes a continuous and dynamic morphogenetic process in a discontinuous manner (only anagen VI and telogen are relatively stable stages; for detailed discussion, see Bernard, 2012). Unlike in scalp skin, anagen I is relatively common in xenografts, making this the model of choice for investigating

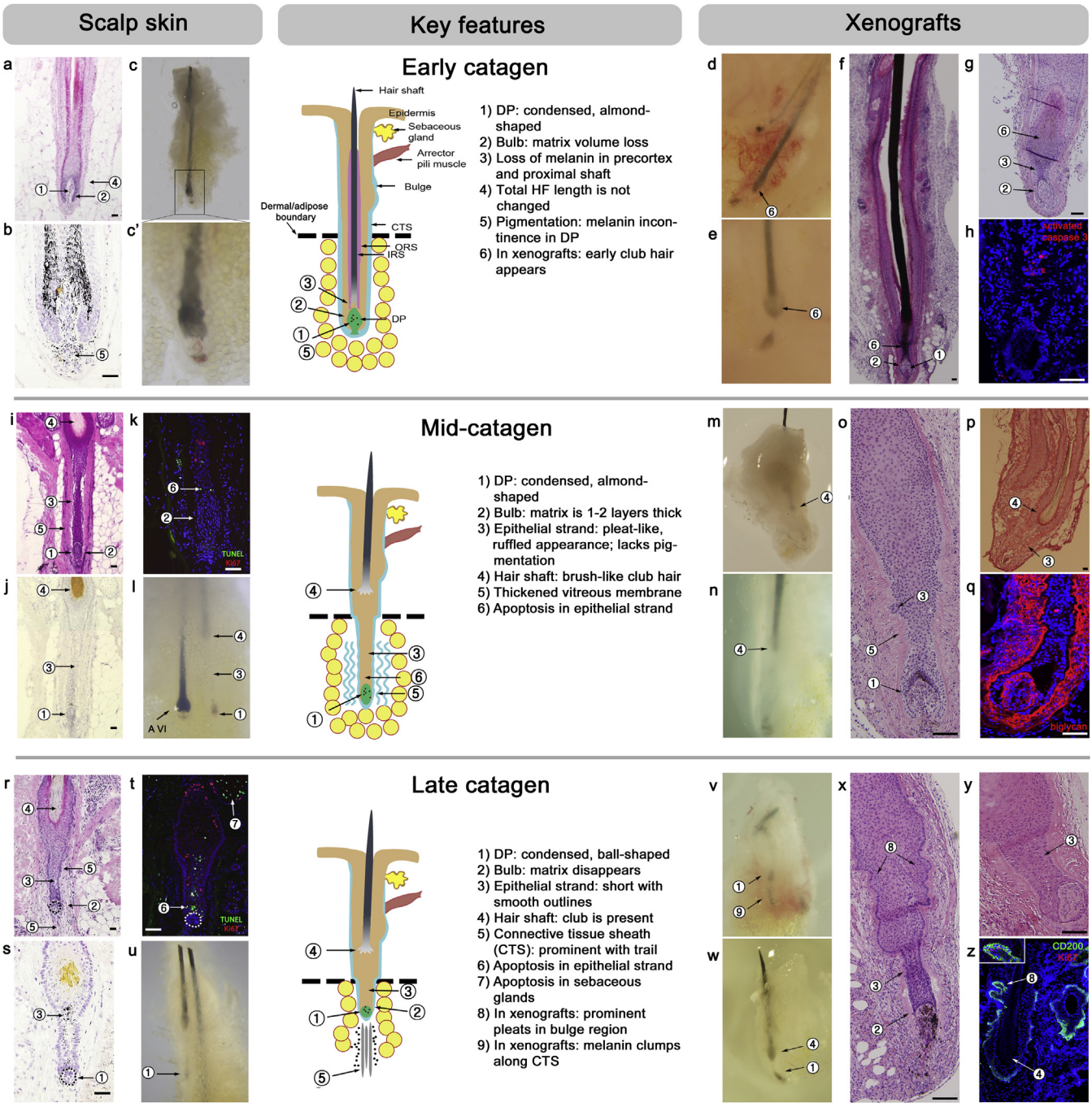

Figure 1. Catagen. For practical reasons, catagen was subdivided into three easily recognizable stages: early, mid-, and late catagen. For each stage, a schematic drawing is provided, with key features numbered and marked. For HFs-IS, 5–10% of all HFs are in catagen. In xenografts, approximately three quarters of HFs-XG undergo "dystrophic catagen," during which a club hair fails to form (see Supplementary Figure S1). (**a**–**h**) Early catagen in HFs-IS (**a**–**c**′) and HFs-XG (**d**–**h**). Key features at this stage are hair matrix volume loss, absence of pigment at the proximal end of the hair shaft, melanin incontinence into the DP, and the appearance of apoptotic cells. On in situ, HF length remains unchanged compared with anagen VI HFs. In xenografts, the peak day for early catagen is postgrafting day 3. (**i**–**q**) Mid-catagen in HFs-IS (**i**–**l**) and HFs-XG (**m**–**q**). Key features at this stage are a shrinking hair matrix, which is only 1–2 cell layers thick, thin epithelial strand with pleated outlines and apoptotic cells, presence of the brush-like club hair, and a thick vitreous membrane. In scalp skin, the proximal portion of the HF is still within the adipose layer. In xenografts, the peak day for mid-catagen is postgrafting day 18. (**r**–**z**) Late catagen in HFs-IS (**r**–**u**) and HFs-XG (**v**–**z**). Key features at this stage are a smaller, ball-shaped DP, absence of the hair matrix, shortened epithelial strand (compared to mid-catagen), prominent connective tissue sheath with the trail below the DP, melanin clumps in the trail, and ongoing apoptosis in the epithelial strand. Additionally, apoptosis occurs in the sebaceous gland in HFs-IS. In xenografts, the bulge region develops prominent pleats. This stage peaks on postgrafting day 29. Hosts: SCID mice (panels **e**, **g**, **m**, **q**, **x**, **y**), nude mice (panels **d**, **f**, **h**, **n**, **o**, **p**, **v**, **w**, **z**). Immunostaining markers: h - activated caspase 3 (red), q - biglycan (red), k, t - TUNEL (green)/Ki67 (red), z - CD200 (green)/Ki67 (red). CTS, connective tissue sheath; DP, dermal papilla; HFs, hair follicles; HFs-IS, hair follicle morphology in human scalp skin in situ; HFs-XG, xenografted anagen hair follicles; IRS, inner root sheath; ORS, outer root sheath; SCID, severe combined immunodeficiency. Scale bars: 100 μm.

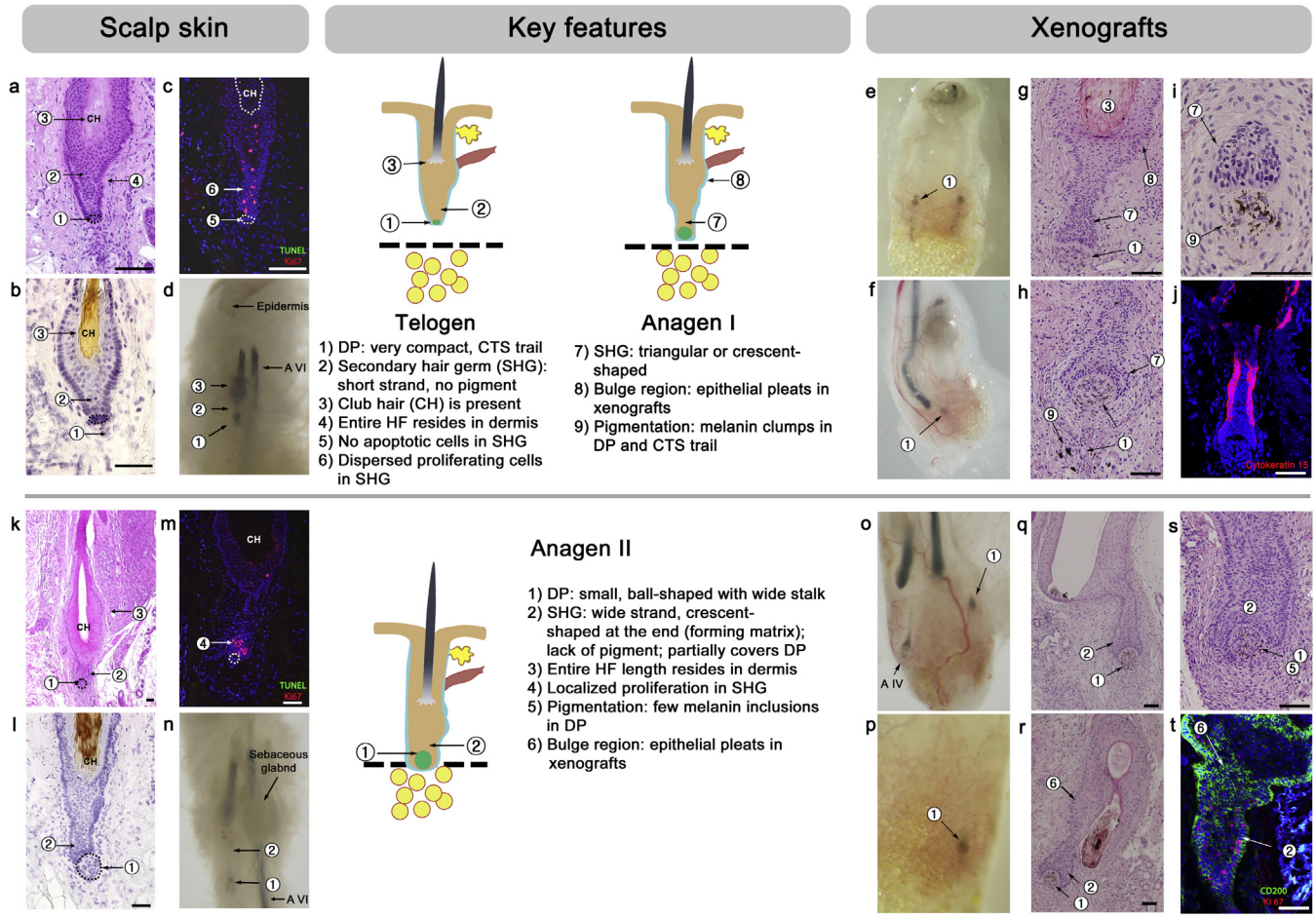

Figure 2. Telogen and anagen I, II. (**a**–**d**) Telogen. HFs with typical telogen morphology represent 1–2% of all HFs on in situ findings and are generally lacking in xenografts. Key features at this stage are a very small DP and a short secondary hair germ that lacks apoptotic cells. The entire length of the telogen HF rests in the dermis. (**e**–**j**) Anagen I. HFs with anagen I morphology are generally not found in situ but are common in xenografts, peaking on postgrafting day 33. Key features at this stage are a small DP, a secondary hair germ shaped as a triangle or a small crescent, and an initiation of proliferation at the base of the germ. (**k**–**t**) Anagen II in HFs-IS (**k**–**n**) and HFs-XG (**o**–**t**). Key features at this stage are a small DP with a wide stalk (compared with telogen and anagen I), an enlarged secondary hair germ with prominent crescent shape, and a localized proliferation hotspot at the base of the germ. On in situ, the entire length of the HF rests in the dermis. In xenografts, the peak day for anagen II is postgrafting day 40. Hosts: SCID mice (panels **f**, **g**, **h**, **j**, **o**, **q**, **r**, **s**), nude mice (panels **e**, **i**, **p**, **t**). Immunostaining markers: c, m - TUNEL (green)/Ki67 (red), j - cytokeratin 15 (red), t - CD200 (green)/Ki67 (red). CH, club hair; CTS, connective tissue sheath; DP, dermal papilla; HFs, hair follicles; HFs-IS, hair follicle morphology in human scalp skin in situ; HFs-XG, xenografted anagen hair follicles; IRS, inner root sheath; ORS, outer root sheath; SCID, severe combined immunodeficiency; SHG, secondary hair germ. Scale bars: 100 μm.

the human telogen-to-anagen transformation. Anagen I HFs-XG display a hybrid morphology: (i) similar to late catagen, their bulge region's epithelium retains a pleated appearance (Figure 2g, feature #8); (ii) the secondary hair germ becomes triangular or crescent-shaped and wraps around the DP (Figure 2g–i, feature #7), which remains condensed and ball-like. DP may contain melanin clumps (i.e., pigment residue from the preceding anagen VI stage) (Figure 2i, feature #9), and still shows a CTS trail (Figure 2h, feature #1).

Anagen II

In HFs-IS and HFs-XG, the secondary hair germ undergoes proliferation-driven thickening and elongation (Figure 2k–t). Its proximal end develops into a new hair matrix that at this stage is still unpigmented, crescent-shaped, and only partially encloses a small, yet slightly larger and less densely packed, ball-shaped DP (Figure 2k and q–s, features #1 and #2). Proliferation markers reveal localized clusters of dividing cells in the thickened hair germ (Figure 2m, feature #4), whereas apoptotic cells are lacking. The entire length of stage II anagen HFs-IS resides above the dermal/adipose boundary. In HFs-XG, the bulge region's epithelium retains its pleated appearance (Figure 2r and t, feature #6), and the DP still contains melanin deposits (Figure 2s, feature #5).

Anagen III

In both HFs-IS and HFs-XG, the hair matrix has now formed and is 4–5 cell layers thick. It encloses at least 60% of the DP, which becomes enlarged and oval-shaped (Figure 3a and g–k, feature #2). Prominently, at this stage, HFs develop a hair shaft and an IRS, both of which are easily identifiable in routine hematoxylin and eosin stains (Figure 3a, b, g, i, and k, feature #3). Immunostaining for proliferation markers reveals actively dividing cells both in the hair matrix and in the ORS (Figure 3c and j, feature #5). In situ, the hair bulb now reaches and extends into the adipose layer. In both HFs-IS and HFs-XG, three anagen III substages can be differentiated

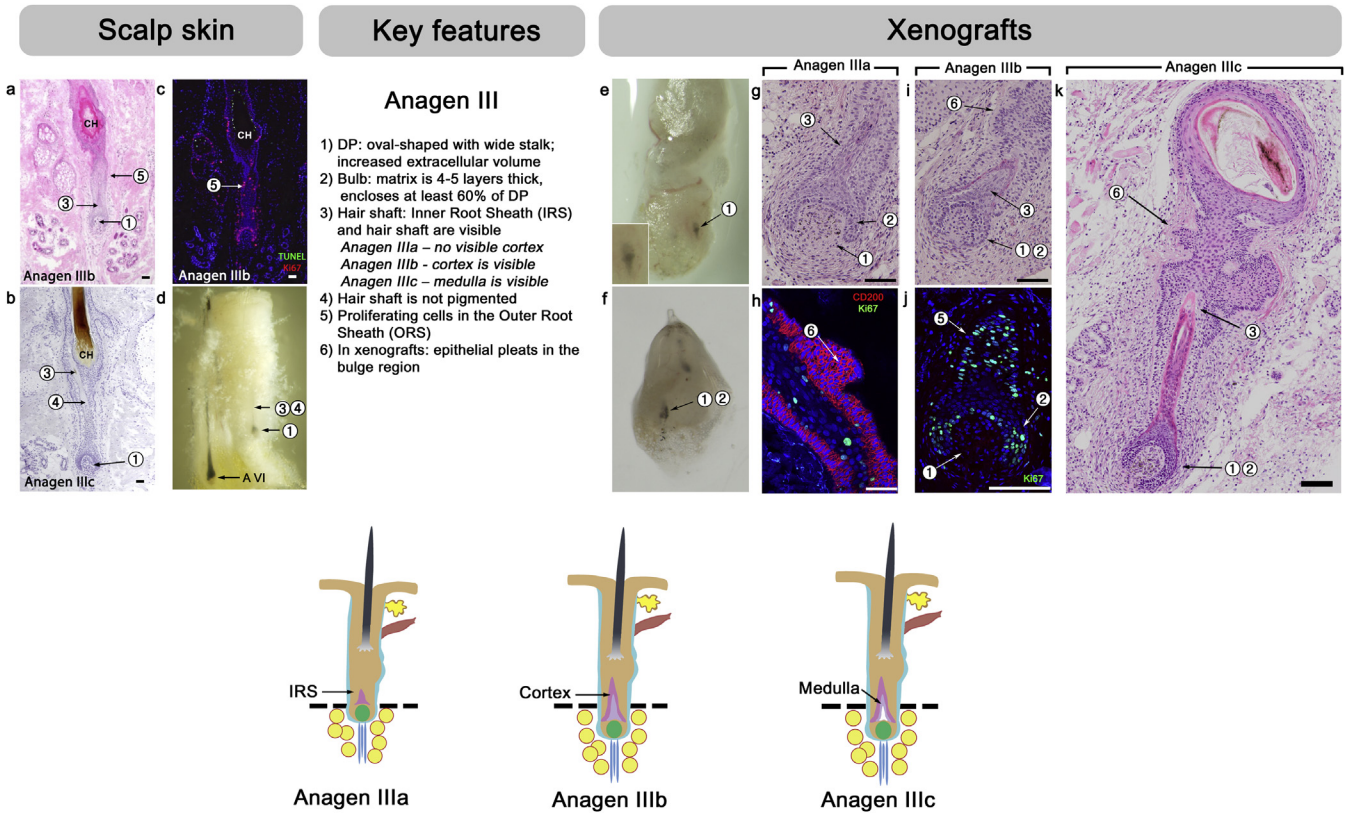

Figure 3. Anagen III. Key features at this stage are an enlarged, oval-shaped DP (compared with anagen II), the presence of a newly formed, albeit small hair matrix (4–5 cell layers thick), small, but visible IRS, and a hair shaft that lacks pigmentation. On in situ, a newly formed hair bulb enters into the adipose layer. Three anagen III substages can be identified on the basis of combined IRS and hair shaft morphology. The bulge region of HFs-XG shows prominent pleats. This stage peaks on postgrafting day 47. Hosts: SCID mice (panels **f**, **h**, **j**), nude mice (panels **e**, **g**, **i**, **k**). Immunostaining markers: c - TUNEL (green)/Ki67 (red), h - Ki67 (green)/CD200 (red), j - Ki67 (green). CTS, connective tissue sheath; DP, dermal papilla; HFs, hair follicles; HFs-IS, hair follicle morphology in human scalp skin in situ; HFs-XG, xenografted anagen hair follicles; IRS, inner root sheath; ORS, outer root sheath; SCID, severe combined immunodeficiency. Scale bars: 100 μm.

based on hair shaft appearance. Anagen IIIa shafts lack a visible cortex (Figure 3g). Anagen IIIb and IIIc shafts have a visible cortex, whereas anagen IIIc hair shafts are long, reaching approximately twice the length of the hair matrix (Figure 3k). Importantly, throughout anagen III, hair shafts still lack visible pigmentation, even though HF melanogenesis in the HF pigmentary unit commences in anagen IIIc (Slominski et al., 2005). Last, the bulge epithelium of HFs-XG retains a pleated appearance (Figure 3i and k, feature #6), and the DP still contains occasional melanin clumps.

Anagen IV

At this stage, the hair shaft is fully mature, with a distinct medulla (in terminal HFs), cortex, and cuticle easily identifiable on hematoxylin and eosin stained sections, and the hair tip reaches the level of the sebaceous gland duct (Figure 4a–h, feature #5). Importantly, melanin production and transfer are now fully reactivated, and hair shafts become visibly pigmented. In situ, the hair bulb now reaches down to the upper dermal adipose layer (Figure 4a, feature #2), and a distinct CTS trail is visible proximal to the bulb, which guides further HF downgrowth (Figure 4a, feature #7).

Anagen V

In situ, the hair bulb extends further into the adipose layer, and the CTS trail disappears at this stage (Figure 4i, feature #2). In both HFs-IS and HFs-XG, the tip of the hair shaft enters the hair canal (Figure 4i, j, and k, feature #5). The DP is now onion-shaped, and in the hair matrix, pigmentation reaches down to Auber's line (Figure 4l and m, features #1, #2, and #6). Additionally, in HFs-XG, bulge epithelium contours begin to smoothen (Figure 4l, feature #8).

Anagen VI

The vast majority of scalp HFs in situ are in anagen stage VI. The hair bulb is located deep in the dermal adipose layer, whereas the hair shaft emerges above the skin level (Figure 4p–w). In pigmented HFs, the hair matrix contains the maximum amount of melanin, which now reaches below Auber's line. In HFs-XG, bulge epithelium smoothens, but residual undulations, which may be homologous to the "follicular trochanter" in HFs-IS (Tiede et al., 2007), can persist (Figure 4u, feature #8). Compared with anagen V, the DP is maximally extended and enriched in extracellular matrix.

Practical recommendations for the xenograft model

Long-term survival of individually grafted human scalp HFs is much more consistent in severe combined immunodeficiency (SCID) mice, averaging between 55% and 67% (Supplementary Figure S6d online). In nude mice, it was extremely variable, ranging from 0% to 82%, likely reflecting mouse-to-mouse variability in graft rejection (Supplementary Figure S4 online). Also, among actively cycling HFs-XG, average hair growth rates are faster and more consistent in

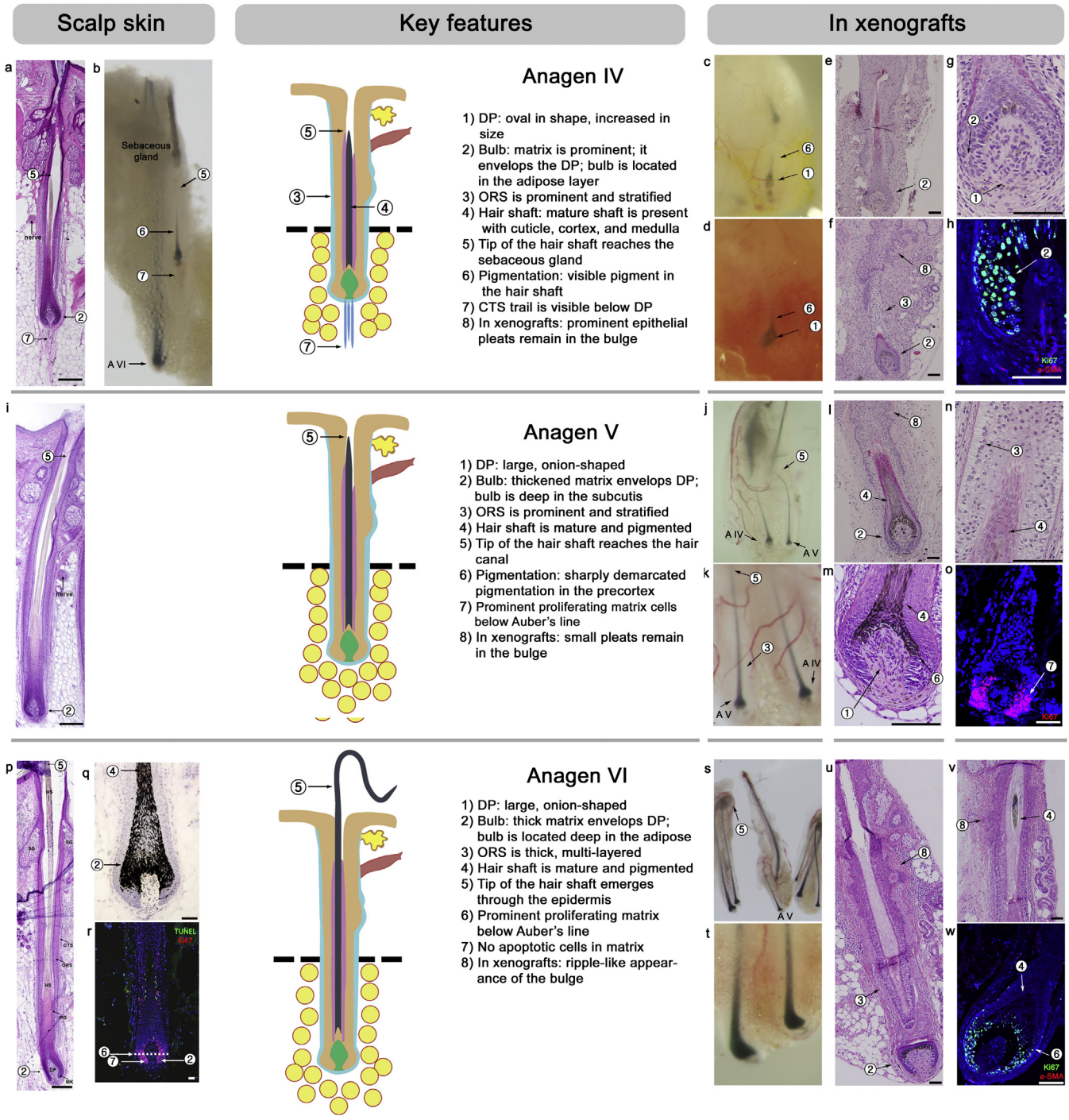

Figure 4. Anagen IV, V, and VI. (**a**–**h**) Anagen IV in HFs-IS (**a**, **b**) and HFs-XG (**c**–**h**). Key features at this stage are a prominent matrix, stratified ORS, and a mature hair shaft that reaches the level of the sebaceous gland. On in situ, the hair bulb is in the adipose layer, but the connective tissue trail can still be seen (it becomes lost during anagen V). HFs-XG IV show prominent pleats in the bulge region and peak on postgrafting day 60. (**i**–**o**) Anagen V in HFs-IS (**i**) and HFs-XG (**j**–**o**). Key features at this stage are a large onion-shaped DP, significantly increased pigmentation (compared with anagen IV) with sharp demarcation at Auber's line, and a mature hair shaft that reaches the hair canal. On in situ, the connective tissue trail disappears (compared with anagen IV). HFs-XG V maintain pleats in the bulge region and peak on postgrafting day 63. (**p**–**w**) Anagen VI in HFs-IS (**p**–**r**) and HFs-XG (**s**–**w**). A total of 90–95% of all HFs-IS are in anagen VI, and all HFs-XG progress to anagen VI by postgrafting day 92. At this stage, HFs achieve their maximum size, and the hair shaft tip extends far above the skin surface. There are no apoptotic cells compared with early catagen. Hosts: SCID mice (panels **e**, **f**, **g**, **m**, **n**, **s**, **t**, **u**, **w**), nude mice (panels **c**, **d**, **h**, **j**, **k**, **l**, **o**, **v**). Immunostaining markers: h, w - Ki67 (green)/alpha smooth muscle actin (red), o - Ki67 (red), r - TUNEL (green)/Ki67 (red). CTS, connective tissue sheath; DP, dermal papilla; HFs, hair follicles; HFs-IS, hair follicle morphology in human scalp skin in situ; HFs-XG, xenografted anagen hair follicles; IRS, inner root sheath; ORS, outer root sheath; SCID, severe combined immunodeficiency. Scale bars: 100 μm.

SCID than in nude mice (Supplementary Figure S6c). This confirms that SCID mice are the host of choice for xenografted human scalp HFs (Gilhar et al., 1998, 2013).

Xenograft transplantation provides a strong stimulus for catagen induction, thereby partially synchronizing hair cycling behavior (Figure 5). However, significant hair cycle

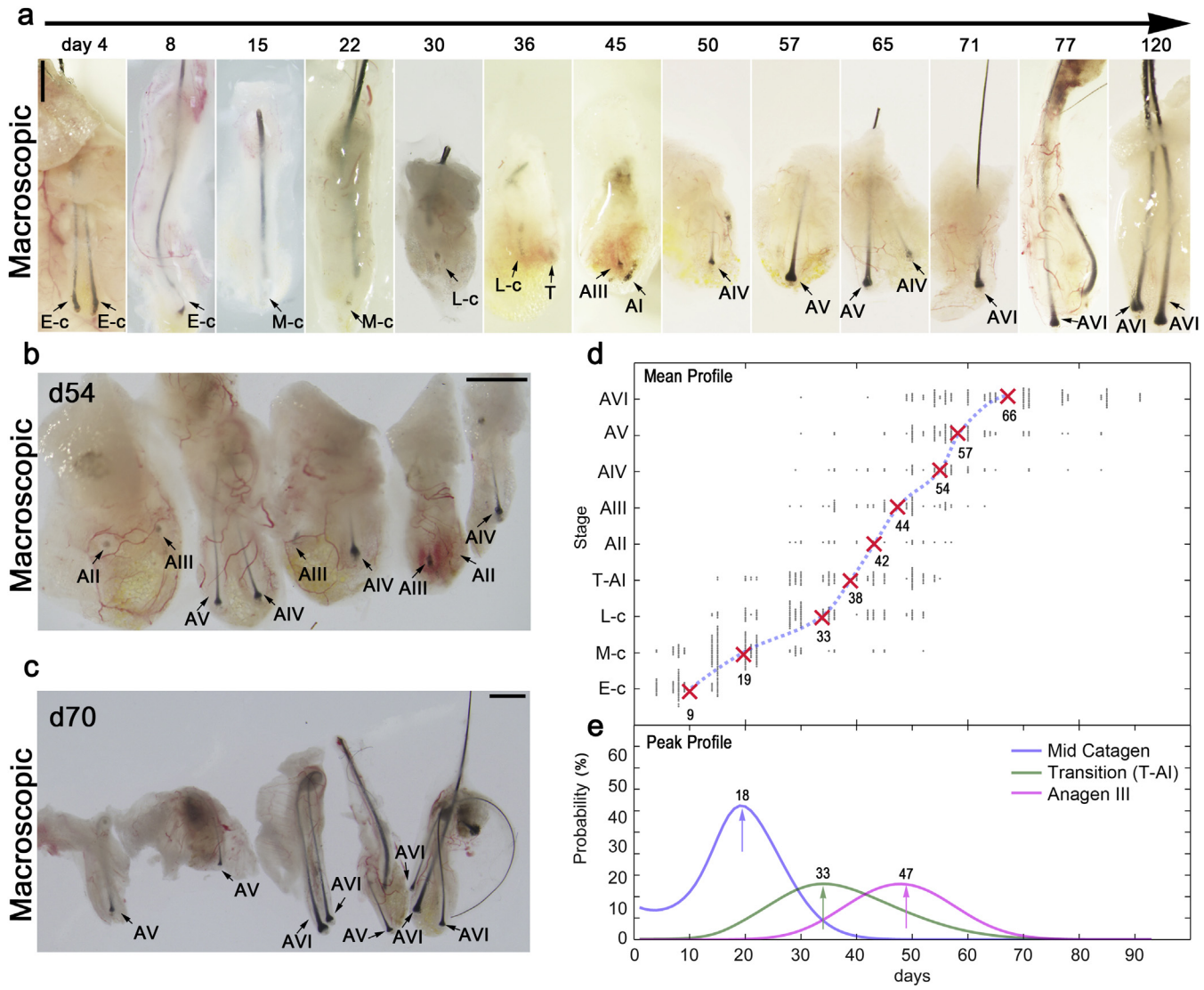

Figure 5. Xenograft model optimization. (**a**) Representative gross morphology of human HFs-XG showing postgrafted hair cycle resetting dynamics: follicles progress through sequential catagen substages, telogen-to-anagen transition stage, and then anagen substages. (**b**, **c**) Representative images showing hair cycle heterogeneity of HFs-XG at days 54 (**b**) and 70 (**c**). (**d**) Comprehensive hair cycle staging of human HFs-XG during the first 90 days (*x*-axis). Average time point values for each substage (*y*-axis) are shown with the average regression curve overlaid over the scatter plot of individual HF stage values (assessed on biopsy; each dot represents one biopsied HF). (**e**) Statistical analysis of the frequency at which the indicated stage appears (early catagen, telogen-to-anagen I transition, and anagen III). The arrows denote the postgrafting time with the greatest probability of selecting HFs-XG at the indicated stage based on the naïve Bayes classifier analysis. Further details (for every hair cycle substage) can be found in Supplementary Figure S5. Hosts: SCID mice (panels **a** [days 15, 22, 50, 57, 65] and **c**), nude mice (panels **a** [days 4, 8, 30, 36, 45, 71, 77, 120] and **b**). HFs, hair follicles; HFs-XG, xenografted anagen HFs; SCID, severe combined immunodeficiency. Scale bars: **a**, **b**, **c**—1 mm.

stage heterogeneity is retained during all postgrafting time points (Figure 5b, c, and d), demonstrating that the mosaicism of human HF cycling is partially maintained even after transplantation. We recommend using statistically adjusted peak time points generated here (see Figure 5e; Supplementary Figure S5 online) to evaluate the postgrafting human hair cycle. Moreover, because the majority of HFs-XG enter anagen stage VI on day 92, studies on anagen should be performed after this time point.

DISCUSSION

Here, we provide a guide for staging terminal human scalp HFs in situ and in xenografts (Supplementary Figure S2 online) on the basis of a minimal set of characteristics, identifiable by routine histology. Depending on the specific hair research question(s) asked, additional standard readout parameters can be employed that make the analysis of human HFs even more instructive, and Supplementary Table S2 lists selected examples for further guidance, including human HF epithelial progenitor markers (Purba et al., 2014, 2015).

The mouse xenotransplant model remains indispensable for studying and experimentally manipulating human HF cycling in vivo. Besides follicular unit transplantation, as in the current study, one can also transplant carefully trimmed full-thickness scalp skin (Gilhar et al., 1998, 2013; Sintov et al., 2000; Van Neste et al., 1989). This greatly reduces the level of surgery-related damage suffered by HFs located

away from the transplant edge and has the added advantage of permitting one to study the cycling behavior of an entire HF field as well as terminal HFs alongside vellus HFs, complete with associated sebaceous and sweat glands. However, perfusion, oxygenation, and reinnervation can be precarious in the center of such full-thickness transplants.

When interpreting data obtained with the xenotransplant model, one must keep in mind a number of confounding factors that may influence the results profoundly. Namely, xenotransplanted human HFs are reperfused and reinnervated by cells and structures derived from an alien host, and are shock-exposed to and must rapidly adjust to the foreign endocrine, innate immune, and metabolic systems of SCID mice. In addition, the murine host launches a stress response to the trauma of surgery (note that perceived stress in mice triggers substantial perifollicular neurogenic inflammation, which is NGF-, substance P-, and mast cell-dependent, centers around the bulge, and prematurely induces catagen in murine anagen HFs (Arck et al., 2005). Coupled with the fact that human scalp HFs also respond to key stress mediators (reviewed in Paus et al., 2014), all of these confounding factors are expected to impact greatly on human HF cycling, growth, immune status, pigmentation, and metabolism in vivo after xenotransplantation. Therefore, caution is advised in extrapolating from observations made with human HF xenotransplants in mice to the response of healthy human scalp skin.

At any given time, the vast majority of asynchronously cycling HFs in healthy human scalp are considered to be in anagen (80–90%), between 10% and 20% in telogen, and only 1–5% in catagen (Dawber, 1997; Shapiro, 2007; Sperling et al., 2012; Whiting, 2004). However, our current histological analysis of HFs-IS suggests that the number of catagen HFs can exceed that of telogen HFs (catagen: 5–10%, telogen: 1–2%). This discrepancy likely reflects differences in assessment methodologies, because phototrichograms cannot distinguish between telogen and catagen and are thus less accurate compared with histology-based hair cycle staging (Hoffmann, 2001; Van Neste and Trueb, 2006). Additional histomorphometric hair cycle staging will be required to refine the true anagen-to-catagen-to-telogen scalp HF ratio.

Because of the relatively short duration of anagen I–V, these anagen stages are rarely found in situ, with the notable exception of the weeks after extensive telogen effluvium, when a surge in premature anagen termination is followed by semisynchronous anagen reactivation (Hadshiew et al., 2004; Harrison and Sinclair, 2002; Katz et al., 2006). Thus, an unusually high percentage of anagen stage I–V HFs points toward a preceding telogen effluvium.

Unlike in situ, anagen I–V HFs can be readily identified in xenografts due to a telogen effluvium-like resetting effect from the traumatic transplantation procedure (Gilhar et al., 1988; Hashimoto et al., 2000, 2001; Jahoda et al., 1996; Van Neste et al., 1989), complicated by various degrees of HF dystrophy, just as after chemotherapy (Paus et al., 1994, 2013). This resetting, however, is incomplete. Although individual xenotransplanted anagen HFs rapidly enter catagen by day 3, their progression through catagen is variable, and late-catagen HFs can still be found on day 50. This likely reflects a variable response to trauma, when some HFs enter into normal, but premature, catagen or the "dystrophic catagen," whereas others undergo a "dystrophic anagen," which protracts catagen development (Hendrix et al., 2005; Paus et al., 2013). This variable timing of the catagen program leads to incomplete hair cycle synchronization, heralding the re-establishment of cycling mosaicism. Additionally, grafted HFs do not appear to enter long-lasting telogen, suggesting that the normal HF stem cell quiescence mechanisms (Geyfman et al., 2014; Mardaryev et al., 2011) may be altered, perhaps as a result of the confounding, host-derived factors summarized above.

SCID mouse xenotransplantation model optimization for studying human anagen

Despite limitations of the xenograft model, HFs-XG closely resemble cycling HFs-IS and are able to enter long-lasting anagen. Therefore, the SCID mouse xenograft model (see also Gilhar et al., 1998, 2013) provides an extremely valuable experimental system for investigating multiple, otherwise difficult-to-study aspects of human HF biology, and instructively complements in vitro human HF and scalp skin organ culture (Al-Nuaimi et al., 2014; Hardman et al., 2015; Kloepper et al., 2010; Langan et al., 2015; Lu et al., 2007; Oh et al., 2013; Philpott et al., 1990; Poeggeler et al., 2010). We recommend using at least three postgrafting time points to study catagen-to-anagen progression, and waiting until after postgrafting 92 days for studying anagen VI HFs. This is substantially later than the postgrafting day 60–70 reported previously (Hashimoto et al., 2000, 2001). Future studies wishing to investigate human HF responses to hormonal stimulation, for example, in the context of androgenetic alopecia, also need to consider the intricate hormone sensitivity of human HFs (Paus et al., 2014) and their keratin expression patterns (Ramot and Paus, 2014); therefore, imitating donor-like hormone levels in host mice (e.g., testosterone) is important (De Brouwer et al., 1997; Krajcik et al., 2003; Sintov et al., 2000; Van Neste et al., 1991).

In summary, although *Mus musculus* remains unrivaled in the insights it has helped to generate into basic HF biology, murine HF physiology is quite different from that of human HF. The xenotransplant model characterized above, therefore, provides an indispensable tool for human preclinical hair research in vivo, if employed together with the comprehensive guide for human hair cycle staging developed here.

MATERIALS AND METHODS

Human scalp hair follicles and xenografting

Institutional approval and written informed patient consent were received for all studies using human tissue samples, and institutional approval was received for all animal studies. Human scalp skin in situ studies were performed on normal occipital and temporal scalp skin samples following previously published protocols (Harries and Paus, 2010; Harries et al., 2013; Kloepper et al., 2010). For xenografting, nonbalding occipital scalp skin specimens were used. The method for human HF xenografting was adapted after Hashimoto et al. (2000). Briefly, 15–40 (on average 25) microdissected anagen VI follicular units were transplanted onto 6- to 8-week-old female nude or SCID mice (Jackson Laboratory, Bar Harbor, ME). A total of 1,164 HFs were transplanted and then biopsied and

analyzed at 45 consecutive time points (see Supplementary Table S3 and Supplementary Materials and Methods online).

Histological tissue analysis

Paraffin embedded HF samples were sectioned at 3 μm thickness, and OCT compound embedded follicles were sectioned at 8 μm at −20 °C. Sections were processed either for routine histology (hematoxylin and eosin staining) or for immunofluorescence staining (see Supplementary Materials and Methods).

Computational analysis and statistical tests

Hair cycle stage's mean date was determined by averaging the time points when biopsied HFs were at the corresponding stage. To estimate the time point with the greatest probability of selecting a HF in the desired stage, the naïve Bayes classifier (Mitchell, 1997) was used. Additional computer simulations were employed to derive probability values for each hair cycle stage, and a two-sample Kolmogorov-Smirnov test (Conover, 1999) was utilized to compare the speed of HFs-XG hair cycle progression between nude and SCID host mice (see Supplementary Materials and Methods for details).

CONFLICT OF INTEREST

The authors state no conflict of interest.

ACKNOWLEDGMENTS

JWO is supported by the Regenerative Medicine R&D fund provided by Daegu city (Korea), and ETRI R&D Program (15ZC3100). MVP is supported by the NIH National Institute of Arthritis and Musculoskeletal and Skin Diseases (NIAMS) grant R01-AR067273, Edward Mallinckrodt Jr. Foundation grant, and the University of California Cancer Research Coordinating Committee (CRCC) grant. This research was also supported by the Basic Science Research Program through the National Research Foundation of Korea (NRF) funded by the Ministry of Education, Science and Technology (NRF-2012R1A1B3001047 to YKS and NRF-2014R1A5A2009242 to MK), and by a grant from Deutsche Forschungsgemeinschaft (Pa 345/13-1) to RP. This research was also supported by Kyungpook National University Research Fund, 2012. The authors are most grateful and indebted to many colleagues, who generously lent a helping hand and/or provided expert advice during some stage of this long-lasting expedition into human hair cycle staging, in particular to Sang In Choi, Chang Hoon Seo, Mi Hee Kwack, Seung Hyun Shin, Sanguk Im, Jin Oh Kim, Dorothee Langan, Koji Sugawara, Nadine Dörwald, Jonathan Le, Manda Nguyen, David Whiting and George Cotsarelis.

SUPPLEMENTARY MATERIAL

Supplementary material is linked to the online version of the paper at www.jidonline.org, and at http://dx.doi.org/10.1038/JID.2015.354.

REFERENCES

Al-Nuaimi Y, Hardman JA, Biro T, et al. A meeting of two chronobiological systems: circadian proteins Period1 and BMAL1 modulate the human hair cycle clock. J Invest Dermatol 2014;134:610−9.

Arck PC, Handjiski B, Kuhlmei A, et al. Mast cell deficient and neurokinin-1 receptor knockout mice are protected from stress-induced hair growth inhibition. J Mol Med (Berl) 2005;83:386−96.

Atanaskova Mesinkovska N, Bergfeld WF. Hair: what is new in diagnosis and management? Female pattern hair loss update: diagnosis and treatment. Dermatol Clin 2013;31:119−27.

Bernard BA. The human hair follicle, a bistable organ? Exp Dermatol 2012;21:401−3.

Bodo E, Tobin DJ, Kamenisch Y, et al. Dissecting the impact of chemotherapy on the human hair follicle: a pragmatic in vitro assay for studying the pathogenesis and potential management of hair follicle dystrophy. Am J Pathol 2007;171:1153−67.

Botchkareva NV, Ahluwalia G, Shander D. Apoptosis in the hair follicle. J Invest Dermatol 2006;126:258−64.

Botchkareva NV, Kahn M, Ahluwalia G, Shander D. Survivin in the human hair follicle. J Invest Dermatol 2007;127:479−82.

Commo S, Bernard BA. Immunohistochemical analysis of tissue remodelling during the anagen-catagen transition of the human hair follicle. Br J Dermatol 1997;137:31−8.

Conover WJ. Practical nonparametric statistics. 3rd edition. New York: Wiley; 1999.

Cotsarelis G. Gene expression profiling gets to the root of human hair follicle stem cells. J Clin Invest 2006;116:19−22.

Courtois M, Loussouarn G, Hourseau C, Grollier JF. Hair cycle and alopecia. Skin Pharmacol 1994;7:84−9.

Crabtree JS, Kilbourne EJ, Peano BJ, et al. A mouse model of androgenetic alopecia. Endocrinology 2010;151:2373−80.

Dawber RPR. Diseases of the hair and scalp. Hoboken, NJ: Wiley; 1997.

De Brouwer B, Tetelin C, Leroy T, Bonfils A, Van Neste D. A controlled study of the effects of RU58841, a non-steroidal antiandrogen, on human hair production by balding scalp grafts maintained on testosterone-conditioned nude mice. Br J Dermatol 1997;137:699−702.

Dry FW. The coat of the mouse (*Mus musculus*). J Gen 1926;16:287−340.

Garza LA, Liu Y, Yang Z, et al. Prostaglandin D2 inhibits hair growth and is elevated in bald scalp of men with androgenetic alopecia. Sci Transl Med 2012;90:1179−96.

Geyfman M, Plikus MV, Treffeisen E, Andersen B, Paus R. Resting no more: redefining telogen, the maintenance stage of the hair growth cycle. Biol Rev Camb Phil Soc 2014.

Gilhar A, Keren A, Shemer A, d'Ovidio R, Ullmann Y, Paus R. Autoimmune disease induction in a healthy human organ: a humanized mouse model of alopecia areata. J Invest Dermatol 2013;133:844−7.

Gilhar A, Pillar T, Etzioni A. The effect of topical cyclosporin on the immediate shedding of human scalp hair grafted onto nude mice. Br J Dermatol 1988;119:767−70.

Gilhar A, Ullmann Y, Berkutzki T, Assy B, Kalish RS. Autoimmune hair loss (alopecia areata) transferred by T lymphocytes to human scalp explants on SCID mice. J Clin Invest 1998;101:62−7.

Hadshiew IM, Foitzik K, Arck PC, Paus R. Burden of hair loss: stress and the underestimated psychosocial impact of telogen effluvium and androgenetic alopecia. J Invest Dermatol 2004;123:455−7.

Halloy J, Bernard BA, Loussouarn G, Goldbeter A. Modeling the dynamics of human hair cycles by a follicular automaton. Proc Natl Acad Sci U S A 2000;97:8328−33.

Hardman JA, Tobin DJ, Haslam IS, et al. The peripheral clock regulates human pigmentation. J Invest Dermatol 2015;135:1053−64.

Harries MJ, Meyer K, Chaudhry I, et al. Lichen planopilaris is characterized by immune privilege collapse of the hair follicle's epithelial stem cell niche. J Pathol 2013;231:236−47.

Harries MJ, Paus R. The pathogenesis of primary cicatricial alopecias. Am J Pathol 2010;177:2152−62.

Harrison S, Sinclair R. Telogen effluvium. Clin Exp Dermatol 2002;27:389−5.

Hashimoto T, Kazama T, Ito M, et al. Histologic and cell kinetic studies of hair loss and subsequent recovery process of human scalp hair follicles grafted onto severe combined immunodeficient mice. J Invest Dermatol 2000;115:200−6.

Hashimoto T, Kazama T, Ito M, et al. Histologic study of the regeneration process of human hair follicles grafted onto SCID mice after bulb amputation. J Investig Dermatol Symp Proc 2001;6:38−42.

Hendrix S, Handjiski B, Peters EM, Paus R. A guide to assessing damage response pathways of the hair follicle: lessons from cyclophosphamide-induced alopecia in mice. J Invest Dermatol 2005;125:42−51.

Higgins CA, Westgate GE, Jahoda CA. From telogen to exogen: mechanisms underlying formation and subsequent loss of the hair club fiber. J Invest Dermatol 2009;129:2100−8.

Hoffmann R. TrichoScan: combining epiluminescence microscopy with digital image analysis for the measurement of hair growth in vivo. Eur J Dermatol 2001;11:362−8.

Hsu YC, Li L, Fuchs E. Emerging interactions between skin stem cells and their niches. Nat Med 2014;20:847−56.

Jahoda CA, Oliver RF, Reynolds AJ, Forrester JC, Horne KA. Human hair follicle regeneration following amputation and grafting into the nude mouse. J Invest Dermatol 1996;107:804−7.

Katz KA, Cotsarelis G, Gupta R, Seykora JT. Telogen effluvium associated with the dopamine agonist pramipexole in a 55-year-old woman with Parkinson's disease. J Am Acad Dermatol 2006;55:S103–4.

Kligman AM. The human hair cycle. J Invest Dermatol 1959;33:307–16.

Kloepper JE, Sugawara K, Al-Nuaimi Y, Gáspár E, van Beek N, Paus R. Methods in hair research: how to objectively distinguish between anagen and catagen in human hair follicle organ culture. Exp Dermatol 2010;19:305–12.

Kloepper JE, Tiede S, Brinckmann J, et al. Immunophenotyping of the human bulge region: the quest to define useful in situ markers for human epithelial hair follicle stem cells and their niche. Exp Dermatol 2008;17:592–609.

Krajcik RA, Vogelman JH, Malloy VL, Orentreich N. Transplants from balding and hairy androgenetic alopecia scalp regrow hair comparably well on immunodeficient mice. J Am Acad Dermatol 2003;48:752–9.

Langan EA, Foitzik-Lau K, Goffin V, Ramot Y, Paus R. Prolactin: an emerging force along the cutaneous-endocrine axis. Trends Endocrinol Metab 2010;21:569–77.

Langan EA, Philpott MP, Kloepper JE, Paus R. Human hair follicle organ culture: Theory, application and perspectives [e-pub ahead of print]. Exp Dermatol 2015. http://dx.doi.org/10.1111/exd.12836 (accessed 18 August 2015).

Lattanand A, Johnson WC. Male pattern alopecia a histopathologic and histochemical study. J Cutan Pathol 1975;2:58–70.

Lindner G, Botchkarev VA, Botchkareva NV, Ling G, van der Veen C, Paus R. Analysis of apoptosis during hair follicle regression (catagen). Am J Pathol 1997;151:1601–17.

Lu Z, Hasse S, Bodo E, Rose C, Funk W, Paus R. Towards the development of a simplified long-term organ culture method for human scalp skin and its appendages under serum-free conditions. Exp Dermatol 2007;16:37–44.

Lyle S, Christofidou-Solomidou M, Liu Y, Elder DE, Albelda S, Cotsarelis G. Human hair follicle bulge cells are biochemically distinct and possess an epithelial stem cell phenotype. J Investig Dermatol Symp Proc 1999;4:296–301.

Malgouries S, Donovan M, Thibaut S, Bernard BA. Heparanase 1: a key participant of inner root sheath differentiation program and hair follicle homeostasis. Exp Dermatol 2008a;17:1017–23.

Malgouries S, Thibaut S, Bernard BA. Proteoglycan expression patterns in human hair follicle. Br J Dermatol 2008b;158:234–42.

Mardaryev AN, Meier N, Poterlowicz K, et al. Lhx2 differentially regulates Sox9, Tcf4 and Lgr5 in hair follicle stem cells to promote epidermal regeneration after injury. Development 2011;138:4843–52.

Mitchell TM. Machine learning. New York: McGraw-Hill; 1997.

Montagna W, Ellis RA. The biology of hair growth. New York, NY: Academic Press; 1958.

Müller-Röver S, Handjiski B, van der Veen C, et al. A comprehensive guide for the accurate classification of murine hair follicles in distinct hair cycle stages. J Invest Dermatol 2001;117:3–15.

Nakamura M, Schneider MR, Schmidt-Ullrich R, Paus R. Mutant laboratory mice with abnormalities in hair follicle morphogenesis, cycling, and/or structure: an update. J Dermatol Sci 2013;69:6–29.

Oh JW, Hsi TC, Guerrero-Juarez CF, Ramos R, Plikus MV. Organotypic skin culture. J Invest Dermatol 2013;133:e14.

Ohnemus U, Uenalan M, Inzunza J, Gustafsson JA, Paus R. The hair follicle as an estrogen target and source. Endocr Rev 2006;27:677–706.

Paus R. Therapeutic strategies for treating hair loss. Drug Discov Today 2006;3:101–10.

Paus R, Cotsarelis G. The biology of hair follicles. N Engl J Med 1999;341:491–7.

Paus R, Foitzik K. In search of the "hair cycle clock": a guided tour. Differentiation 2004;72:489–511.

Paus R, Handjiski B, Eichmüller S, Czarnetzki BM. Chemotherapy-induced alopecia in mice. Induction by cyclophosphamide, inhibition by cyclosporine A, and modulation by dexamethasone. Am J Pathol 1994;144:719–34.

Paus R, Haslam IS, Sharov AA, Botchkarev VA. Pathobiology of chemotherapy-induced hair loss. Lancet Oncol 2013;14:e50–9.

Paus R, Langan EA, Vidali S, Ramot Y, Andersen B. Neuroendocrinology of the hair follicle: principles and clinical perspectives. Trends Mol Med 2014;20:559–70.

Philpott MP, Green MR, Kealey T. Human hair growth in vitro. J Cell Sci 1990;97(Pt 3):463–71.

Plikus MV, Baker RE, Chen CC, et al. Self-organizing and stochastic behaviors during the regeneration of hair stem cells. Science 2011;332:586–9.

Plikus MV, Chuong CM. Macroenvironmental regulation of hair cycling and collective regenerative behavior. Cold Spring Harb Perspect Med 2014;4:a015198.

Plikus MV, Mayer JA, de la Cruz D, et al. Cyclic dermal BMP signalling regulates stem cell activation during hair regeneration. Nature 2008;451:340–4.

Poeggeler B, Bodó E, Nadrowitz R, Dunst J, Paus R. A simple assay for the study of human hair follicle damage induced by ionizing irradiation. Exp Dermatol 2010;19:e306–9.

Purba TS, Haslam IS, Poblet E, et al. Human epithelial hair follicle stem cells and their progeny: current state of knowledge, the widening gap in translational research and future challenges. BioEssays 2014;36:513–25.

Purba TS, Haslam IS, Shahmalak A, Bhogal RK, Paus R. Mapping the expression of epithelial hair follicle stem cell-related transcription factors LHX2 and SOX9 in the human hair follicle. Exp Dermatol 2015;24:462–7.

Ramot Y, Paus R. Harnessing neuroendocrine controls of keratin expression: a new therapeutic strategy for skin diseases? BioEssays 2014;36:672–86.

Rebora A, Guarrera M. Kenogen. A new phase of the hair cycle? Dermatology 2002;205:108–10.

Schneider MR, Schmidt-Ullrich R, Paus R. The hair follicle as a dynamic miniorgan. Curr Biol 2009;19:R132–42.

Shapiro J. Clinical practice. Hair loss in women. N Engl J Med 2007;357:1620–30.

Sharova TY, Poterlowicz K, Botchkareva NV, et al. Complex changes in the apoptotic and cell differentiation programs during initiation of the hair follicle response to chemotherapy. J Invest Dermatol 2014;134:2873–82.

Sintov A, Serafimovich S, Gilhar A. New topical antiandrogenic formulations can stimulate hair growth in human bald scalp grafted onto mice. Int J Pharm 2000;194:125–34.

Slominski A, Wortsman J, Plonka PM, Schallreuter KU, Paus R, Tobin DJ. Hair follicle pigmentation. J Invest Dermatol 2005;124:13–21.

Sperling LC, Cowper SE, Knopp EA. An atlas of hair pathology with clinical correlations. 2nd edition. New York, NY: Taylor & Francis; 2012.

Stenn K. Exogen is an active, separately controlled phase of the hair growth cycle. J Am Acad Dermatol 2005;52:374–5.

Sundberg JP, Beamer WG, Uno H, Van Neste D, King LE. Androgenetic alopecia: in vivo models. Exp Mol Pathol 1999;67:118–30.

Sundberg JP, Peters EM, Paus R. Analysis of hair follicles in mutant laboratory mice. J Investig Dermatol Symp Proc 2005;10:264–70.

Tang L, Madani S, Lui H, Shapiro J. Regeneration of a new hair follicle from the upper half of a human hair follicle in a nude mouse. J Invest Dermatol 2002;119:983–4.

Tiede S, Kloepper JE, Whiting DA, Paus R. The 'follicular trochanter': an epithelial compartment of the human hair follicle bulge region in need of further characterization. Br J Dermatol 2007;157:1013–6.

Tobin DJ. The cell biology of human hair follicle pigmentation. Pigment Cell Melanoma Res 2011;24:75–88.

Unger WP. Hair transplantation: current concepts and techniques. J Investig Dermatol Symp Proc 2005;10:225–9.

Van Neste D, De Brouwer B, Dumortier M. Reduced linear hair growth rates of vellus and of terminal hairs produced by human balding scalp grafted onto nude mice. Ann N Y Acad Sci 1991;642:480–2.

Van Neste D, Trueb RM. Critical study of hair growth analysis with computer-assisted methods. J Eur Acad Dermatol Venereol 2006;20:578–83.

Van Neste D, Warnier G, Thulliez M, Van Hoof F. Human hair follicle grafts onto nude mice: morphological study. In: Van Neste D, Lachapelle JM, Antoine JL, editors. Trends in human hair growth and alopecia research. Dordrecht, the Netherlands: Springer; 1989. p. 117–31.

Van Neste MD. Assessment of hair loss: clinical relevance of hair growth evaluation methods. Clin Exp Dermatol 2002;27:358–65.

Whiting DA. The structure of the human hair follicle: light microscopy of vertical and horizontal sections of scalp biopsies. NJ: Canfield Publishing; 2004.